Design of a Wearable Three-Channel Transthoracic Bioimpedance Spectroscopy Front-End with Synchronized ECG Acquisition

Abu Bony Amin[1], *Graduate Student Member, IEEE*, Ebenezer Asabre[1], Yeonsik Noh[1, 2], *Member, IEEE*
[1]*Department of Electrical and Computer Engineering*
[2]*Elaine Marieb College of Nursing*
University of Massachusetts Amherst
Amherst, MA, USA
abubonyamin@umass.edu, easabre@umass.edu, ynoh@umass.edu

***Abstract*—Transthoracic bioimpedance spectroscopy is a promising wearable sensing modality for tracking impedance-based physiological changes, but practical wearable acquisition is limited by the lack of synchronized cardiac electrical information. This paper presents a portable three-channel thoracic bioimpedance front-end with synchronized electrocardiogram acquisition. The system integrates a DDS based sinusoidal excitation source, single-supply analog conditioning, a Tietze-type VCCS, multiplexed tetrapolar electrode selection, lead-off detection, GPD, an ECG analog front-end, microcontroller control, Bluetooth communication, and battery-powered operation. The excitation circuit generates 100 frequency points from 1 kHz to 1 MHz with an approximately $290\mu A$ current and less than 5 percent variation across the measured band. Based on the evaluated data, the impedance mean absolute percentage errors were $3.9\pm0.24\%$, $5.2\pm0.32\%$, and $5.72\pm0.5\%$ for Channels 1–3, respectively. The corresponding phase mean absolute errors were $1.12\pm0.5^{\circ}$, $1.08\pm0.7^{\circ}$, and $1.4\pm0.65^{\circ}$. Position-matched Nyquist trajectories further confirmed preservation of the resistive and reactive impedance components for all three channels. The integrated ECG path produced clearly identifiable $R-peaks$ over a $30s$ recording. These results demonstrate a compact, single-supply platform capable of acquiring validated multi-frequency BioZ data from all three transthoracic paths together with synchronized cardiac electrical timing.**

***Index Terms*—transthoracic bioimpedance spectroscopy, electrocardiography, wearable sensor, voltage-controlled current source, gain and phase detection, tetrapolar electrodes, multi-channel acquisition**

I. Introduction

Transthoracic bioimpedance spectroscopy (TBIS) has emerged as an attractive sensing modality for non-invasive and wearable physiological monitoring because electrical impedance changes can reflect tissue composition, fluid distribution, and cardiac-related impedance variation. Recent reviews of wearable BioZ interfaces emphasize that BioZ sensors are well suited for long-term monitoring because they are non-invasive, low-cost, and user friendly; however, they also identify major circuit-level challenges, including low-noise readout, large baseline impedance, electrode–tissue impedance, motion artifacts, common-mode interference, safety-limited current injection, and low-power operation for battery-powered devices [1].

Multi-frequency measurement provides information than a single-frequency BioZ measurement because tissue resistance and capacitive behavior vary across frequency. Groenendaal et al. described transthoracic BioZ as containing both static tissue information and dynamic physiological variation, while Schoutteten et al. demonstrated the feasibility of semi-continuous, multi-frequency thoracic BioZ measurements during changes in fluid status [2], [3]. These studies support the use of spectroscopy rather than a single impedance when the objective is to preserve resistance, reactance, phase, and frequency-dependent trends for physiological interpretation.

ECG provides complementary information because it directly measures cardiac electrical activity and supplies a temporal reference for heart rate, beat-to-beat intervals, and impedance-related cardiac changes. Recent wearable systems have therefore combined transthoracic impedance with ECG, heart rate, and motion sensing [4], [5]. The System for Heart Failure Identification Using an External Lung Fluid Device (SHIELD) study further showed that combining transthoracic BioZ with ECG-derived heart-rate-variability features improved fluid-status classification, illustrating the potential value of synchronized electrical and impedance-based measurements [6]. Acquiring both signals within one device also avoids timestamp uncertainty and additional hardware associated with separate BioZ and ECG instruments.

A clinically useful wearable platform must first produce technically reliable data. For BioZ, this requires a controlled AC excitation current, accurate magnitude and phase extraction, and reduced sensitivity to the electrode interface. Tetrapolar sensing separates current injection from voltage measurement and thereby reduces electrode–tissue impedance contamination compared with a two-electrode configuration [1], [7]. Nevertheless, a single transthoracic path remains vulnerable to local contact variation, garment pressure, electrode displacement, and motion. Prior wearable fluid-accumulation-vest (FAV) studies demonstrated the feasibility of home-based transthoracic BioZ acquisition, but sufficient usable data were not obtained from every enrolled participant, highlighting the continuing need for improved acquisition robustness [8].

This work addresses these limitations through a 3-channel

This work was supported by the National Heart, Lung, and Blood Institute (NHLBI) of the National Institutes of Health (NIH) under Award Number R01HL165009. The content is solely the responsibility of the authors and does not necessarily represent the official views of the NIH.

transthoracic architecture in which all channels are designed to provide valid, position-specific impedance spectra. Each tetrapolar path measures a different thoracic region and is evaluated against a reference analyzer measurement obtained at the same electrode location. The architecture therefore provides spatially distributed transthoracic information while allowing channel-specific signal-quality assessment. Path 1 additionally supports synchronized one-lead ECG acquisition, enabling cardiac timing and impedance spectroscopy within a common MCU-controlled platform. The main contributions of this work are: 1) a wearable three-channel TBIS front-end that acquires valid spectra from all paths using a shared excitation and readout chain; 2) stable approximately 290 μA excitation across $1kHz$–$1MHz$; 3) channel-wise validation against position-matched analyzer references; and 4) synchronized ECG acquisition within the same portable platform.

II. SYSTEM OVERVIEW

Fig. 1 shows the complete concept of the proposed wearable TBIS–ECG platform. The system consists of a compact bioimpedance and ECG electronics module connected to a thoracic vest containing three tetrapolar electrode paths. Each bioimpedance path contains two current-injection electrodes and two voltage-sensing electrodes. This tetrapolar configuration is used because the current-injection path is separated from the voltage-sensing path, reducing the effect of electrode–tissue impedance on the measured BioZ signal. This design choice is consistent with wearable BioZ interface literature, which notes that two-electrode BioZ measurements suffer from electrode–tissue impedance contamination, while four-electrode measurements improve BioZ accuracy by separating current flow from voltage measurement [1].

The three-channel architecture is not intended to measure unrelated body regions. Instead, all channels focus on the thoracic area, with each channel observing a slightly different transthoracic path. This is important because prior wearable fluid-accumulation vest (FAV) studies showed that daily transthoracic bioimpedance can be measured at home and transmitted using a mobile-phone system, but reliable acquisition remains a practical limitation. In the FAV-mobile phone dyad observational study, 106 participants completed follow-up; however, the prediction algorithm was evaluated only among participants with sufficient FAV data, n = 57, highlighting the need for improved wearable data quality and acquisition robustness [8].

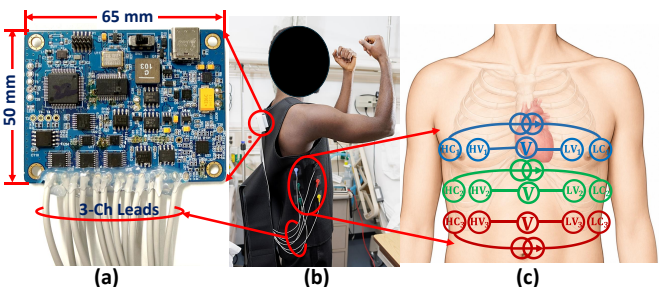

Fig. 1. Overview of the proposed wearable three-channel TBIS and ECG acquisition system. (a) Prototype PCB with dimensions of 65 mm × 50 mm. (b) Vest with the electronics module packaged in an 80 mm × 60 mm × 20 mm enclosure. (c) Three tetrapolar transthoracic electrode paths, while Path 1, positioned closest to the heart, also provides the electrode interface for synchronized one-lead ECG acquisition.

III. CIRCUIT AND SYSTEM ARCHITECTURE

Fig. 2 presents the complete circuit architecture. The system is organized into six major blocks: excitation generation, current injection, electrode/channel selection, gain/phase readout, synchronized ECG acquisition and data transmission through bluetooth. The measurement sequence begins with lead-off detection to verify electrode contact. Once valid connections are confirmed, the MCU sequentially selects each transthoracic channel and controls the DDS frequency sweep; the resulting excitation drives the VCCS, while the measured gain and phase outputs are digitized by the MCU and continuously transmitted via Bluetooth to a smartphone for real-time display and storage throughout the 5 min acquisition period.

A. DDS-Based Frequency Generation

The signal chain begins with a programmable DDS source. BioZ spectroscopy requires controlled excitation at multiple frequencies. In this device, the DDS block provides programmable sinusoidal excitation over 100 frequency points from 1 kHz to 1 MHz The circuit was designed with additional high-frequency margin up to 1.5 MHz to reduce the uncertainty that the useful 1 MHz range operates at the edge of the analog bandwidth.

The circuit uses an AD9851BRSZ DDS controlled by the MCU through Word Load Clock (W_CLK), Frequency Update/Chip Select (FQ_UD), Master Reset (RESET), and Serial Data Input (SDI) signals. DDS excitation enables repeatable MCU-controlled stepped-frequency sine-wave generation while simplifying synchronization of frequency updates, MUX selection, and ADC sampling.

B. Single-Supply Excitation and VCCS Current Generation

After the frequency-programmable sinusoidal waveform is generated by the DDS, the analog excitation chain operates

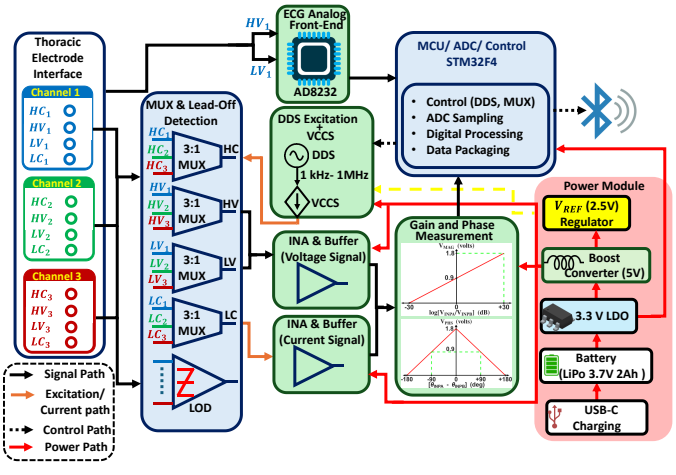

Fig. 2. Circuit and system architecture of the proposed three-channel TBIS–ECG platform which integrates DDS-based excitation, post-DDS filtering and buffering, a single-supply Tietze-type VCCS, MUX-based tetrapolar path selection, lead-off detection, gain and phase readout, an ECG analog front-end, MCU-based timing and control, Bluetooth communication, and battery-powered regulation. The MCU coordinates electrode-contact verification, channel selection, frequency stepping, data acquisition, and continuous transmission to a smartphone during the measurement period.

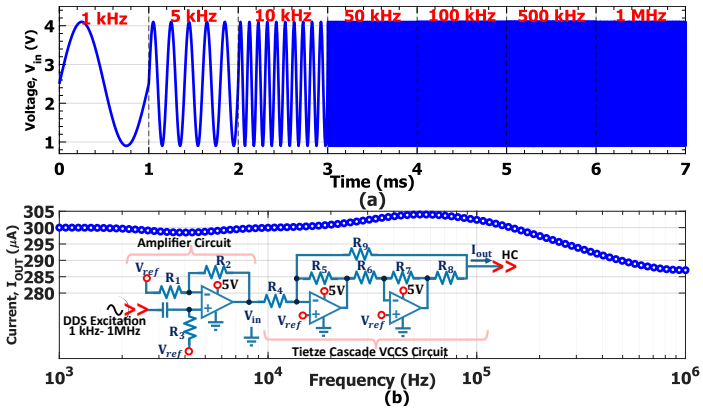

Fig. 3. Single-supply excitation conditioning and VCCS current-generation performance. (a) Representative DDS-generated sinusoidal waveforms centered at the 2.5 V mid-supply reference for single +5 V operation at selected frequencies from the 100-point sweep between 1 kHz and 1 MHz. (b) Tietze-type VCCS design condition and measured output current across frequency.

from a single +5-V supply, eliminating the need for a negative rail. This simplifies portable implementation by reducing the regulator count, board area, circuit complexity, and power loss, which is advantageous for battery-powered wearable systems.

To enable single-supply operation, the excitation signal is AC-coupled and re-biased around a 2.5-V mid-supply reference, V_{ref}, which serves as the local analog virtual ground, as shown in Fig. 3(a). The AC-coupling capacitor blocks DC offsets from the DDS and preceding stages, thereby preventing unintended DC current from reaching the VCCS and electrode interface. Because V_{ref} establishes the common-mode level of the analog chain, it is generated using a low-noise, well-decoupled reference to minimize errors in the measured impedance magnitude and phase.

The filtered, buffered, AC-coupled, and biased sinusoidal voltage is then applied to a Tietze-type voltage-controlled current source (VCCS), which generates an approximately 290 μA AC excitation current for transthoracic BioZ measurement. Because impedance is determined from the injected current and the resulting sensed voltage, the VCCS must maintain a stable current magnitude with minimal phase distortion over the 1 kHz–1 MHz operating range. The measured frequency-dependent current response of the implemented VCCS is presented in Fig. 3(b).

C. Multiplexed Tetrapolar Electrode Interface and GPD

The electrode interface uses a multiplexed architecture to select among three transthoracic BioZ paths while sharing a single excitation and readout chain. Each path contains four electrodes: HC and LC for current injection, and HV and LV for voltage sensing. The schematic includes the path-specific nodes HC_1–HC_3, LC_1–LC_3, HV_1–HV_3, and LV_1–LV_3. The selected current-injection and voltage-sensing paths are controlled by the MCU.

For each selected path, an AC current is injected through the outer electrode pair, while the resulting transthoracic voltage is measured through the inner electrode pair. This tetrapolar configuration reduces the influence of electrode–tissue interface impedance because the current-injection and voltage-sensing paths are separated, as illustrated in Fig. 3(c). The sensed voltage is subsequently routed to the gain/phase detector (GPD) for impedance estimation [9], [10].

D. Lead-Off and Poor-Contact Detection

Lead-off detection is included because a three-channel system is only useful if the device can identify whether each channel is electrically reliable. The lead-off block functioned as a fault-aware measurement layer as it is shown in Fig. 2. It helps classify whether the transthoracic path is likely usable, degraded, or invalid. The circuit converts electrode-contact uncertainty into an explicit system variable. This is a central system-level advantage over single-channel BioZ monitors, where one poor contact might invalidate the entire recording.

IV. RESULTS AND DISCUSSION

A. VCCS Current Stability, and Single-Supply Operation

Table I summarizes the principal limitations of representative VCCS architectures and the corresponding mitigation strategies adopted in the proposed design. As shown in Fig. 3(b), the implemented VCCS maintains an excitation current close to the target value of 290 μA throughout the 100-point frequency sweep from 1 kHz to 1 MHz, with a deviation of less than 5% near the upper end of the frequency range. This variation is primarily attributed to the reduction in op-amp loop gain and effective VCCS output impedance at higher frequencies. Nevertheless, the excitation current remains sufficiently stable for impedance extraction across the proposed transthoracic BioZ measurement range.

B. Three-Channel Impedance and Phase Accuracy

20 healthy male participants completed the study with [mean $\pm$ SD]: age, (19.2 $\pm$ 1.2) yrs; height, 173.5 $\pm$ 6.8 cm; body mass, 69.4 $\pm$ 8.7 kg. BioZ measurements from the proposed device were validated against a Zurich Instruments MFIA impedance analyzer and precision LCR meter (500 kHz/5 MHz). All participants provided written informed consent after being informed of the procedures and potential risks. The study was approved by the University of Massachusetts Amherst Institutional Review Board (#22040451).

Fig. 4 evaluates the impedance-measurement accuracy of the proposed device across the three transthoracic channels. Measurements from each channel were compared with a position-matched BioZ analyzer reference acquired at the correspond-

TABLE I
CURRENT-SOURCE LIMITATIONS AND PROPOSED DESIGN RESPONSE

Current-source approach	Reported limitation	Proposed design response
Enhanced Howland current source [11]	Output impedance and current flatness degrade at high frequency due to resistor mismatch, op-amp nonlinearities, and stray capacitance.	Compact Tietze-type VCCS with measured current validation over 1 kHz–1 MHz.
Conventional dual Howland current source [12]	Stray capacitance at op-amp inputs, switches, and output nodes affects current accuracy above 100 kHz.	Short analog routing, filtered DDS drive, and parasitic-aware implementation.
Compensated Howland/load-in-loop designs [12]	Improved high-frequency current stability but increased circuit complexity.	Simpler wearable-oriented VCCS with stable current under single-supply operation.
High-voltage or dual-supply VCCS [13]	Requires additional rails or converters, increasing power and hardware complexity.	Single +5 V supply with a 2.5 V analog reference for battery-compatible operation.

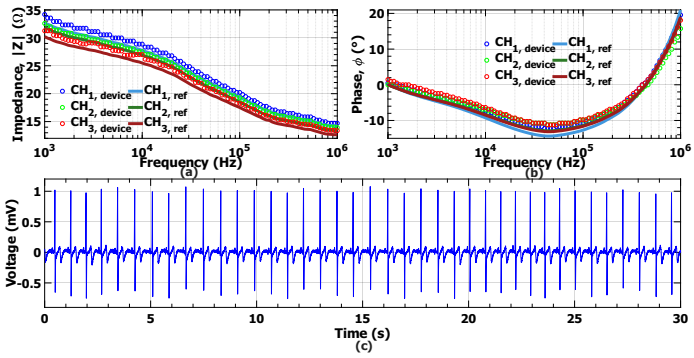

Fig. 4. Three-channel TBIS-ECG acquisition. (a) Impedance measured by the proposed device for CH1, CH2, and CH3 compared with the position-matched BioZ-analyzer reference for each channel. (b) Corresponding device and position-matched reference phase responses. (e) Representative 30 s one-lead ECG waveform acquired from Path 1 at a sampling rate of 1 kHz.

ing electrode location. Therefore, the reported errors represent device-to-reference agreement for each thoracic path rather than physiological differences among electrode placements.

As shown in Fig. 4(a), the measured impedance magnitude closely follows the corresponding analyzer reference for all three channels. Across the 1 kHz–1 MHz frequency sweep, the impedance magnitude decreases from approximately 30–33 Ω at the low-frequency end to approximately 13–15 Ω at the high-frequency end. The phase responses shown in Fig. 4(b) also reproduce the corresponding reference trends. The phase begins near 0° at 1 kHz, decreases to approximately -10° to -12° in the mid-frequency region, and subsequently increases to approximately 15°–20° near 1 MHz.

Table II summarizes the impedance-magnitude mean absolute percentage error (MAPE) and phase mean absolute error (MAE) calculated over the 100-point frequency sweep. The noticeable higher magnitude error and intermeasurement spread observed for Ch3 may partly reflect its lower thoracic placement, which is farther from the heart and more strongly influenced by the lower lung region. Compared with the upper thoracic paths, this location may exhibit greater anatomical and posture-dependent variability and may be more sensitive to small variations in electrode contact and current-path distribution. Consequently, modest differences between the device and position-matched reference can produce a comparatively larger relative error in Ch3. Nevertheless, all three channels demonstrate close agreement with their corresponding references, supporting the accuracy of the proposed multichannel acquisition system over the intended BioZ frequency range.

C. Synchronized ECG Acquisition

Fig. 4(c) shows a representative 30 s ECG waveform acquired using the integrated ECG path. The signal is centered near 0 mV, with visible R-peaks reaching approximately 0.9–1.0 mV and negative deflections around -0.6 to -0.8 mV. The clear R-peak morphology confirms that the Path-1 electrode configuration can acquire usable one-lead ECG while the same device performs thoracic BioZ acquisition. This is important because ECG provides direct electrical cardiac timing, while BioZ provides impedance-based physiological information. Since both signals are acquired within the same MCU-controlled platform, the system avoids the timing uncertainty that would occur if ECG and BioZ were recorded using separate instruments.

TABLE II
BIOZ MEASUREMENT ERROR ACROSS FREQUENCY POINTS PER SUBJECT

Channel	Impedance MAPE (%)	Phase MAE (degree)
Ch1	3.9 ± 0.24	1.12 ± 0.5
Ch2	5.2 ± 0.32	1.08 ± 0.7
Ch3	5.72 ± 0.5	1.4 ± 0.65

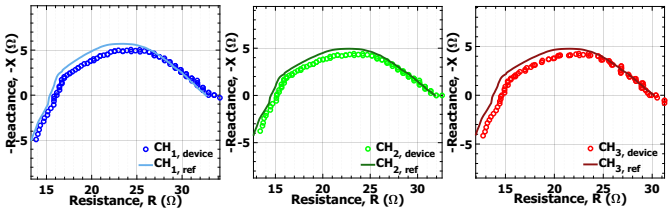

Fig. 5. Channel-wise Nyquist validation of the measured complex transthoracic impedance. Nyquist trajectories of (a) Ch1, (b) Ch2, and (c) Ch3 compared with the respective position-matched bioimpedance-analyzer references.

D. Nyquist Analysis of Complex Impedance

Fig. 5 presents the Nyquist trajectories of Ch1, Ch2, and Ch3, with each device response compared against its position-matched BioZ-analyzer reference. Across all three channels, the measured trajectories closely follow the corresponding reference arcs, demonstrating agreement in both the resistive and reactive components of the transthoracic impedance.

The Ch1 and Ch2 trajectories span resistance ranges of approximately 14–32 Ω, whereas the Ch3 trajectory spans approximately 12–31 Ω. For each channel, the trajectory rises to a maximum negative-reactance value, $-X$, of approximately 5 Ω in the mid-frequency region before returning toward the resistive axis at higher frequencies. This arc-shaped behavior demonstrates that the system captures the frequency-dependent capacitive response of the corresponding thoracic paths. Although the Ch3 device trajectory exhibits slightly greater separation from its position-matched reference, consistent with the higher impedance-magnitude MAPE and phase MAE reported in Table II, its overall trajectory and curvature remain well aligned with the reference. These results demonstrate that the proposed system preserves the complex-impedance trajectories of all three transthoracic channels. The resistance and reactance components provide complementary information regarding the frequency-dependent electrical characteristics of each measurement path.

V. CONCLUSION

Overall, the proposed architecture shifts transthoracic BioZ acquisition from a single-path measurement approach toward a multi-path, fault-aware wearable sensing platform. By combining three tetrapolar transthoracic BioZ paths, lead-off-aware channel assessment, and synchronized ECG acquisition, the system improves the opportunity to obtain usable physiological data when one electrode path is degraded. Future work will extend the platform toward signal-quality-aware ML by combining multi-channel TBIS features, Cole-Cole parameters, ECG-derived HRV features, and channel-quality indicators for transthoracic fluid-status assessment and worsening-HF prediction.

REFERENCES

[1] J. Xu and Z. Hong, "Low power bio-impedance sensor interfaces: Review and electronics design methodology," *IEEE Reviews in Biomedical Engineering*, vol. 15, pp. 23–35, 2022.

[2] W. Groenendaal, S. Lee, and C. Van Hoof, "Wearable bioimpedance monitoring: Viewpoint for application in chronic conditions," *JMIR biomedical engineering*, vol. 6, no. 2, p. e22911, 2021.

[3] M. K. Schoutteten, L. Lindeboom, H. De Cannière, Z. Pieters, L. Bruckers, A. D. Brys, P. Van der Heijden, B. De Moor, J. Peeters, C. Van Hoof *et al.*, "The feasibility of semi-continuous and multi-frequency thoracic bioimpedance measurements by a wearable device during fluid changes in hemodialysis patients," *Sensors*, vol. 24, no. 6, p. 1890, 2024.

[4] S. M. Iqbal, I. Mahgoub, E. Du, M. A. Leavitt, and W. Asghar, "Development of a wearable belt with integrated sensors for measuring multiple physiological parameters related to heart failure," *Scientific reports*, vol. 12, no. 1, p. 20264, 2022.

[5] A. M. Hughes, D. J. Taylor, P. D. Morris, and E. L. Brittain, "Wearable devices and cardiovascular health: revolutionizing remote monitoring and disease prevention," *European Heart Journal*, vol. 47, no. 18, pp. 2130–2145, 2026.

[6] N. Reljin, H. F. Posada-Quintero, C. Eaton-Robb, S. Binici, E. Ensom, E. Ding, A. Hayes, J. Riistama, C. Darling, D. McManus *et al.*, "Machine learning model based on transthoracic bioimpedance and heart rate variability for lung fluid accumulation detection: prospective clinical study," *JMIR Medical Informatics*, vol. 8, no. 8, p. e18715, 2020.

[7] E. Piuzzi, S. Pisa, E. Pittella, L. Podestà, and S. Sangiovanni, "Low-cost and portable impedance plethysmography system for the simultaneous detection of respiratory and heart activities," *IEEE Sensors Journal*, vol. 19, no. 7, pp. 2735–2746, 2019.

[8] C. E. Darling, S. Dovancescu, J. S. Saczynski, J. Riistama, F. S. Kuniyoshi, J. Rock, T. E. Meyer, and D. D. McManus, "Bioimpedance-based heart failure deterioration prediction using a prototype fluid accumulation vest-mobile phone dyad: an observational study," *JMIR cardio*, vol. 1, no. 1, p. e6057, 2017.

[9] B. Ben Atitallah, A. Y. Kallel, D. Bouchaala, N. Derbel, and O. Kanoun, "Comparative study of measurement methods for embedded bioimpedance spectroscopy systems," *Sensors*, vol. 22, no. 15, p. 5801, 2022.

[10] K. Ain, F. Chandra, Q. Zaka, B. Fahrani, A. Amelia, A. F. Enggar, R. Rulaningtyas, L. Muqmiroh, and B. Ariwanto, "Design of bioimpedance spectroscopy to characterize meat based on gain and phase detector (ad8302)," in *2021 International Conference on Instrumentation, Control, and Automation (ICA)*, 2021, pp. 55–59.

[11] T. Menden, J. Matuszczyk, S. Leonhardt, and M. Walter, "Bandwidth and common mode optimization for current and voltage sources in bioimpedance spectroscopy," *Journal of Electrical Bioimpedance*, vol. 12, no. 1, p. 135, 2021.

[12] H. Nouri, D. Bouchaala, Y. Zhao, A. Y. Kallel, and O. Kanoun, "Load in the loop dual howland current source for wide frequency bandwidth and wide load range bioimpedance measurements," *IEEE Transactions on Instrumentation and Measurement*, vol. 73, pp. 1–10, 2024.

[13] C. Ouni, B. Ghoul, H. Al-Shaikhli, J. Ma'touq, A. Fakhfakh, and O. Kanoun, "A low-power voltage-controlled current source for wearable bioimpedance applications," in *2025 IEEE 22nd International Multi-Conference on Systems, Signals & Devices (SSD)*, 2025, pp. 551–556.